Global aspects of the energy landscape of metastable crystal structures in ionic compounds

1999 J. Phys.: Condens. Matter 11 6487

(http://iopscience.iop.org/0953-8984/11/33/316)

J. Phys.: Condens. Matter **11** (1999) 6487–6499. Printed in the UK PII: S0953-8984(99)02095-0

Global aspects of the energy landscape of metastable crystal structures in ionic compounds

M A C Wevers, J C Schön and M Jansen

Max-Planck-Institut für Festkörperforschung, Heisenbergstrasse 1, D-70569 Stuttgart, Germany

Received 24 February 1999

Abstract. Understanding the properties of complex systems requires the analysis of their energy landscape. Using simple models for the crystalline compounds MgF_2 and CaF_2 as example landscapes, we show that, in addition to the construction of tree-graph approximations of the landscape, the threshold algorithm can be employed to calculate local densities of states for regions of the landscape around local minima, and to determine the probabilities of transitions between such minima. This information is then correlated with the results of global optimizations and relaxations.

1. Introduction

Studying the energy landscapes of complex systems is crucial to understanding many aspects of their behaviour [1, 2], ranging from the relaxation dynamics in glasses [3–5] and spin glasses [6, 7], the folding transition in proteins [8–11], the success of combinatorial optimization procedures [12, 13], the properties of clusters [14] and polymers [15], to the question of the very existence and stability of crystalline compounds [16–18]. A number of techniques [19–25] have been employed to explore the energy hypersurface of multi-minima systems, with special emphasis on the detection of local minima and the determination of the energy barriers separating them. Besides other results, these techniques have been used to construct highly simplified representations of the energy landscape, in particular, the construction of single-lump tree graphs [26] (also called e.g. disconnection trees [27], disconnectivity graphs [15] or 1D projections [28]), where basins around local minima of the energy landscape are represented as nodes of a tree graph.

However, this picture is in most instances too simplified to allow a description of e.g. the temperature-dependent dynamics of the system. Using the lid algorithm [12, 29], it has been found for a number of discrete energy landscapes like those of spin glasses [7, 30], lattice networks [31], or the travelling salesman problem [12] that it is necessary to take both the local density of states, and the way the basins are connected into account. The former influences e.g. the dynamic stability of the basin, while the latter (sometimes called the 'entropic' barrier structure) together with the energetic barriers controls the rate of transition between two local minima and their equilibration. These stability aspects are of greatest importance for the existence of metastable crystalline compounds: a (meta)stable compound corresponds to a locally ergodic region R of the energy landscape [18], where the equilibration time within R is considerably shorter than the escape time, and shorter than or comparable to the observation time, $\tau_{eq} < t_{obs} \ll \tau_{esc}$. In previous work, we have employed the so-called threshold algorithm [26] to construct a more refined version of the single-lump trees mentioned above,

0953-8984/99/336487+13$30.00

where the basins are represented by a sequence of nodes weighted by the number of states within energy slices. As was shown by Hoffmann, Sibani and co-workers [32], random walks on such weighted trees can be used to represent the relaxation dynamics of complex systems.

In this paper, we go beyond the purely energetic aspects of the energy landscape. Starting from a number of deep-lying local minima of the potential energy of two example systems, we have used the threshold algorithm to determine the energetic barriers between these local minima, the local densities of states of the individual basins, and the transitions between the basins for sequences of prescribed energy lids. These quantities can be represented by so-called transition maps, and we find that they are correlated with the results of global optimization procedures used to determine local minima of the energy landscapes. As examples, we have chosen (computationally accessible) simplified models of two related crystalline systems, MgF_2 and CaF_2, with two formula units in a periodically repeated simulation cell, where the energy is calculated via a two-body interaction potential between the ions.

2. Model and computational aspects

Analysing the energy landscape of a solid globally is a highly non-trivial task, and even with modern computers available it is necessary to employ a number of radical simplifications to achieve this task. Thus, we have introduced periodic boundary conditions, and we employ two formula units ($z = 2$) of atoms per simulation cell. Furthermore, we use a simple empirical two-body interaction potential between the atoms consisting of a Coulomb and a Lennard-Jones term, in order to allow for fast calculations of the energy of a given configuration [33]. For the systems MgF_2 and CaF_2 ($z = 2$), the Lennard-Jones parameters were $\epsilon(MgF_2) = 0.3$ eV/atom and $\epsilon(CaF_2) = 0.4$ eV/atom, respectively. Furthermore, $\sigma_{ij} = R_i + R_j$, where R_i is the radius of ion i ($R_{Mg^{2+}} = 0.78$ Å, $R_{Ca^{2+}} = 1.06$ Å, $R_{F^{1-}} = 1.33$ Å). The Coulomb energy was calculated by a method using Ewald summation as proposed by deLeeuw *et al* [34]. In the context of this model, the total energy was calculated within 10^{-3} eV/atom.

In earlier work [33], many local minima for the energy landscapes of these systems had been determined using simulated annealing. In the present work, these minima served as starting points for so-called threshold runs: starting from a minimum x_i, random walks were performed (85% and 15% of the moves were changes of relative coordinates and cell vectors, respectively), where only moves which did not exceed a sequence of prescribed energy lids L_k were accepted (the lids were usually spaced in energy by 0.1 eV/atom). During such a random walk, periodically quenches (usually every 5×10^4 or every 10^4 steps, each with a length of 10^4 steps) were performed, in order to check whether a barrier to some other minimum had been crossed. The lowest lid value where this occurs constitutes an upper bound on the actual energy barrier between these two minima. From this, we constructed tree graphs approximating the energy landscape (cf. figure 1). During the analysis of the threshold results, many new local minima were detected that had not been encountered during the initial global optimization. Due to the limited computation time not all local minima have been used as starting configurations of threshold runs; however, because of the very low total frequency of occurrence and relatively high energy of the omitted minima, they were very unlikely to represent important structure candidates. A list of the most important structure candidates encountered when investigating MgF_2 and CaF_2 is given in table 1. In order to gather some rudimentary statistics, the random walk was repeated for five seed values of the random-number generator, for each lid value and starting minimum.

In addition, the energy of the states was sampled (every 100th step) during each run, yielding a distribution $n(E; L_k, x_i)$ that is approximately proportional to the local density of states $g(E; L_k, x_i)$ in the pocket below the lid L_k. However, due to the very fast (approximately

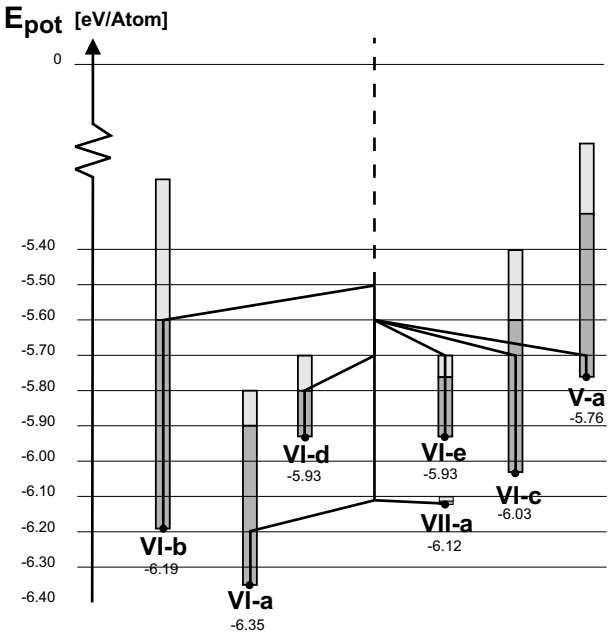

(a)

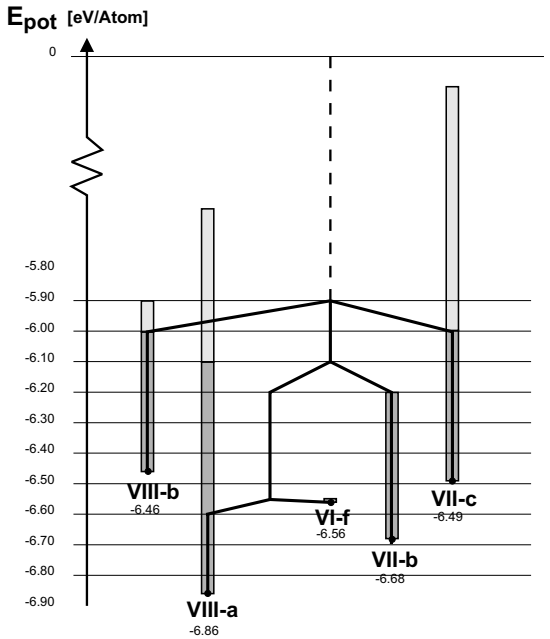

(b)

Figure 1. Tree-graph diagrams. For description of the minima cf. table 1. Connections of lines mark lid values where a transition to other minima is found for the first time. The heights of the bars on the minima indicate the energies up to which 100% (dark) and 80% (light) of the threshold runs ended at the starting minimum. (a) MgF_2, (b) CaF_2.

Table 1. Crystallographic data for the (idealized) minima. The symmetry analysis was performed using the programs SFND [38] and RGS [39].

Minimum	Space group (crystal system)	Cell constants a, b, c (Å); α, β, γ	Atom	x	y	z
Rutile	$P4_2/mnm$ (136),	$a = 4.608, b = 4.608, c = 3.007$	F (4f)	0.300	0.300	0
VI-a	tetragonal	$\alpha = 90.00, \beta = 90.00, \gamma = 90.00$	Mg (2a)	0	0	0
Anatase	$I4_1/amd$ (141),	$a = 3.897, b = 3.897, c = 9.089$	F (8e)	0	1/4	0.595
VI-b	origin choice 2, tetragonal	$\alpha = 90.00, \beta = 90.00, \gamma = 90.00$	Mg (4b)	0	1/4	3/8
VII-a	$Pmn2_1$ (31)	$a = 3.287, b = 4.999, c = 3.713$	F1 (2a)	0	0.427	0.368
	orthorhombic	$\alpha = 90.00, \beta = 90.00, \gamma = 90.00$	F2 (2a)	0	0.935	0.811
			Mg (2a)	0	0.764	0.308
VI-c	$P4/mmm$ (123),	$a = 2.870, b = 2.870, c = 3.824$	F1 (1d)	1/2	1/2	1/2
	tetragonal	$\alpha = 90.00, \beta = 90.00, \gamma = 90.00$	F2 (1c)	1/2	1/2	0
			Mg (1a)	0	0	0
CdI_2	$P\bar{3}m1$ (164),	$a = 3.088, b = 3.088, c = 4.017$	F (2d)	1/3	2/3	0.727
VI-d	trigonal	$\alpha = 90.00, \beta = 90.00, \gamma = 120.00$	Mg (1b)	0	0	1/2
VI-e	$Cmc2_1$ (36),	$a = 2.913, b = 6.718, c = 6.685$	F1 (4a)	0	0.003	0.297
	orthorhombic	$\alpha = 90.00, \beta = 90.00, \gamma = 90.00$	F2 (4a)	0	0.717	0.553
			Mg (4a)	0	0.294	0.750
V-a	$P12_1/m1$ (11),	$a = 8.038, b = 3.882, c = 6.000$	F1 (2e)	0.250	1/4	0.250
	monoclinic	$\alpha = 90.00, \beta = 81.00, \gamma = 90.00$	F2 (2e)	0.901	1/4	0.475
			F3 (2e)	0.250	1/4	0.750
			F4 (2e)	0.599	1/4	0.025
			Mg1 (2e)	0.144	1/4	0.518
			Mg2 (2e)	0.356	1/4	0.982
Fluorite	$I4/mmm$ (139),	$a = 3.831, b = 3.831, c = 5.414$	Ca (4d)	0	1/2	1/4
VIII-a	tetragonal	$\alpha = 90.00, \beta = 90.00, \gamma = 90.00$	F (2a)	1/2	1/2	1/2
		cubic setting:				
		$a = b = 5.418, c = 5.414$				
VII-b	$Cmcm$ (63),	$a = 3.469, b = 7.789, c = 5.482$	Ca (4c)	0	0.104	1/4
	orthorhombic	$\alpha = 90.00, \beta = 90.00, \gamma = 90.00$	F1 (4c)	0	0.798	1/4
			F2 (4b)	0	1/2	0
$CaCl_2$	$Pnnm$ (58),	$a = 4.536, b = 5.646, c = 3.569$	F(4g)	0.230	0.167	0
VI-f	orthorhombic	$\alpha = 90.00, \beta = 90.00, \gamma = 90.00$	Ca (2b)	0	0	1/2
VII-c	$Amm2$ (38),	$a = 3.393, b = 3.104, c = 7.842$	F1 (2b)	1/2	0	0.612
	orthorhombic	$\alpha = 90.00, \beta = 90.00, \gamma = 90.00$	Ca (2b)	1/2	0	0.326
			F2 (2a)	0	0	0.879
VIII-b	$P4/mmm$ (123),	$a = 3.732, b = 3.732, c = 2.873$	F (2e)	0	1/2	1/2
	tetragonal	$\alpha = 90.00, \beta = 90.00, \gamma = 90.00$	Ca (1a)	0	0	0

exponential; cf. figure 3, later) increase in $g(E)$, one obtains sufficient statistics only for energies close to the current lid. Thus, we need to use the overlap between $n(E; L_k, x_i)$ for the sequence of lids L_k, to reconstruct the density of states of the pocket, up to a normalization factor [26].

One should note several aspects of these local densities of states (d.o.s.). Firstly, only for systems with large numbers of atoms/simulation cell can these local d.o.s. yield good quantitative approximations of the vibrational d.o.s. of the real (infinite) system. Secondly,

unless the pocket is very small and devoid of internal structure, 'entropic' barriers within the pocket can influence the outcome of the sampling. Thus, the statistical sampling yields an effective local d.o.s. that represents the local entropy of the region of the energy landscape that is accessible during the finite random walks. Of great relevance for the relaxation dynamics and kinetic stability of the local minima is the inverse slope of nearly linear pieces in the semi-logarithmic plot of the local d.o.s., since this is proportional to the so-called 'trapping temperature' T_c [12, 13]. While for $T > T_c$, the probability for finding an (allowed according to the Metropolis criterion [35]) state with higher energy during an MC run is larger than that of finding those states that are lower in energy due to the exponentially growing number of states, this probability scenario is abruptly reversed for $T < T_c$. Therefore, for $T < T_c$ the system is trapped in the pocket of the landscape, while for $T > T_c$, this region is practically invisible to the random walker. Together, the sampling effect and potential of trapping constitute a strong dynamical aspect of the local d.o.s. Finally, there can occur shifts in the d.o.s. at energy values where very large side-basins of the landscape are added. In figure 3 (see later) such shifts are not depicted, because they are only of minor relevance for the dynamics of the system compared to the slope of the d.o.s.

Since the random walks are of finite length l_r (usually 2.5×10^5 or 5×10^4 steps), there is a non-zero probability that the system will not reach a certain minimum x_j, even if there exists a path below the current lid between x_i and x_j. This transition probability $t_{ji}(L_k; l_r)$ is approximately given by the number of successful transitions from x_i to x_j. In order to visually represent the transition probabilities, we construct so-called transition maps (see figure 2). Each minimum region is represented as a circle, and the energy of the minimum is indicated by the shade of grey. Minimum regions that appear to be extended over a large volume of configuration space are depicted as ovals. The percentage within the circles refers to the probability (summed over all lids) with which runs starting at a given minimum ended up in that minimum at the finish of the threshold run. (This is also referred to in the tree graphs, where the 'lid' value up to which the quench runs reach the starting minimum exclusively (100% 'returns') is indicated by a dark bar, while lightly shaded bars indicate that the starting minimum was reached in over 80% of all quench runs.) The size (in per cent) of the transition probabilities into neighbouring minima is represented by arrows of various sizes and colours. The relative barrier height $L_{rel}(x_i \rightarrow x_j) = L(x_i \rightarrow x_j) - E_0(x_i)$ for the lowest transition found from x_i to x_j is coded in the colours of the arrows. For a better overview two diagrams for the transitions are drawn, one for transition probabilities equal to or above 5%, and one for those below 5%.

The threshold runs presented here took about one year of CPU time on several HP9000-735 workstations. For more technical details on various aspects of the threshold runs—the identification of minima regions, the influence of the lengths of threshold runs, the construction of the transition maps and the densities of states, and the statistical aspects of the results—see reference [36].

3. Results

3.1. MgF_2

In the MgF_2 system the most important new local minima found during the threshold runs were anatase and a number of structures containing prisms as coordination polyhedra (cf. table 1). Note that only the 'prism' structure VI-e with the highest frequency of occurrence has been used as a starting configuration. Some of the rarer local minima (percentage of occurrences in all threshold runs for each minimum $<1\%$) lie in subregions with an energy range of

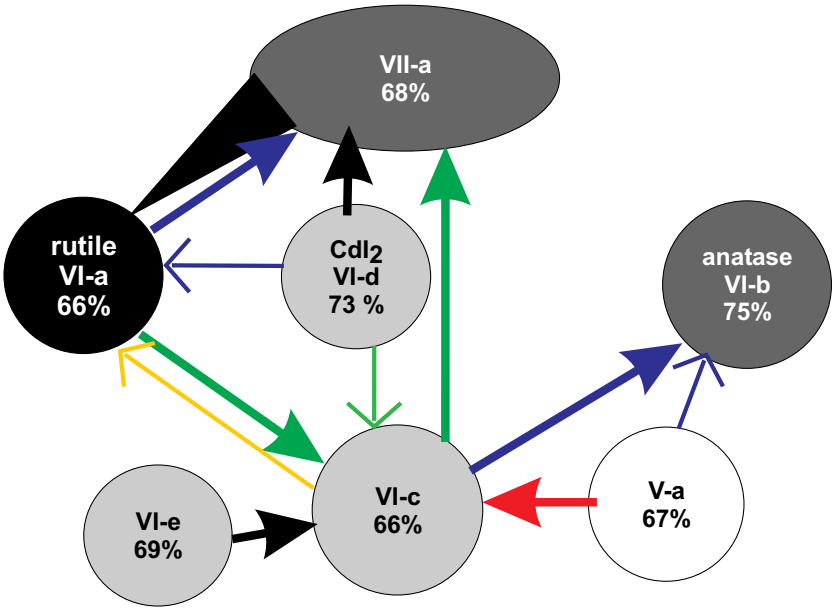

(a)

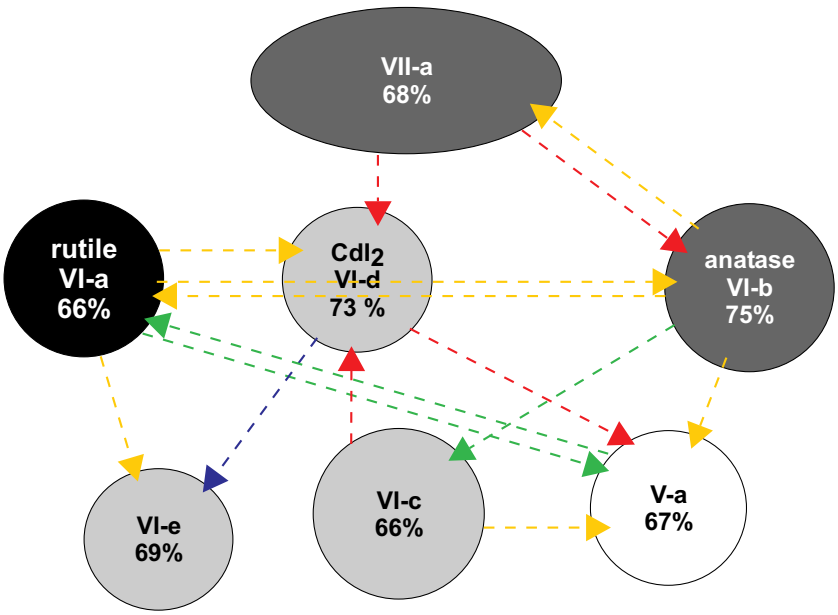

(b)

Figure 2. Transition maps. Transitions from minimum A to minimum B are depicted as arrows of various sizes depending on the frequency of occurrence: $\geqslant$20%: triangular arrows; $\geqslant$10%: bold tips and lines; $\geqslant$5%: plain tips and lines; $<$5%: dotted lines. Transitions $\geqslant$5% and $<$5% are shown in (a)/(c) and (b)/(d), respectively. Minima are represented by circles with their 'return' probability (see the text) given in per cent. Relative barrier heights (in eV/atom) L_{rel} for the transitions (see the text) and energies (in eV/atom) of the minima E_{min} are coded in colours and greyscales of the arrows and circles, respectively. (a)/(b) MgF_2. Energy scale for E_{min}: black: $\leqslant -6.2$; dark grey: $\leqslant -5.9$; light grey: $\leqslant -5.7$; white: $\leqslant -5.5$. Energy scale for L_{rel}: black: $\leqslant$0.4; blue: $\leqslant$0.6; green: $\leqslant$0.8; yellow: $\leqslant$1.2; red: $>$1.2. (c)/(d) CaF_2. Energy scale for E_{min}: black: $\leqslant -6.8$; dark grey: $\leqslant -6.6$; light grey: $\leqslant -6.4$. Energy scale for L_{rel} as for MgF_2.

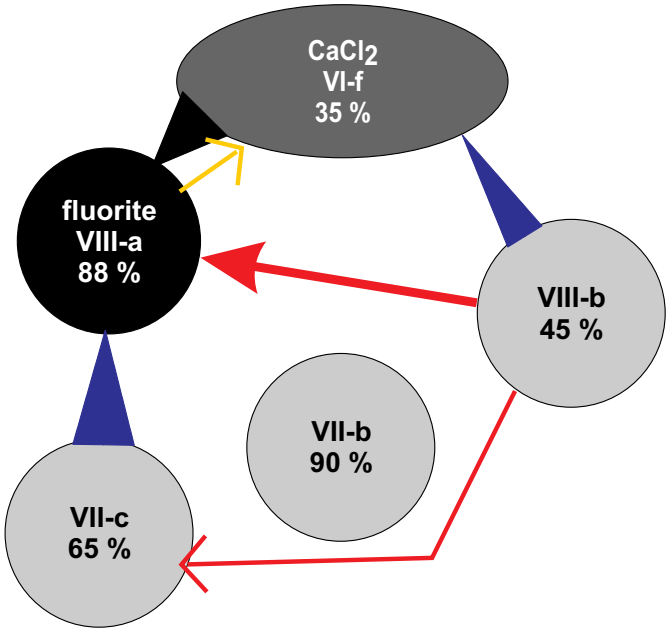

(c)

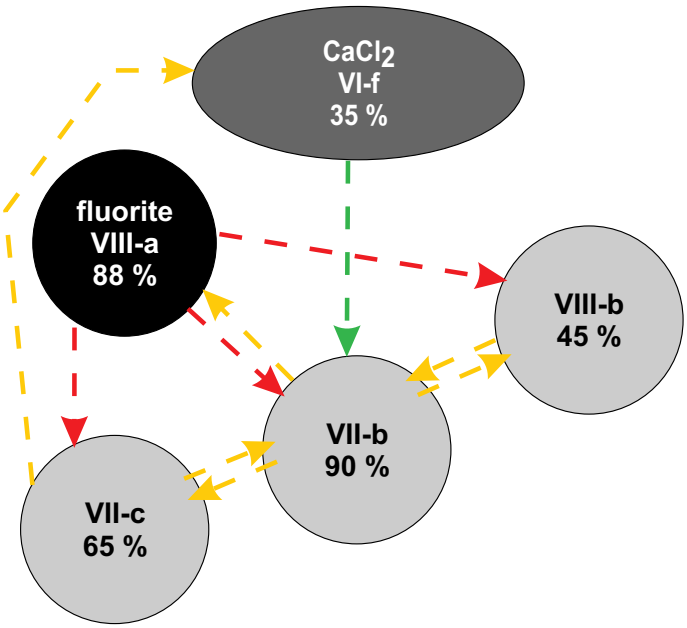

(d)

Figure 2. (Continued)

-5.200 to -5.500 eV/atom (coordination number, $CN = 4, 5$) and -5.550 to -5.900 eV/atom ($CN = 5, 6$). No specific information about the details of the barrier structure within these

regions is available from the present threshold runs.

The diagrams 1a and 2a/b for MgF_2 show some important features. The two energetically lowest minima are VI-a (rutile) and VI-b (anatase). On the route from higher-energy regions to the rutile minimum there lies a sevenfold-coordinated structure VII-a, which exhibits the smallest energy barrier in this system. There are found high probabilities of transitions between VII-a and VI-a. However, the transition from VI-a to VII-a is not observed for $L < -5.8$ eV/atom, whereas the first transition from VII-a to VI-a already occurs at $L = -6.105$ eV/atom. In contrast, VI-b is connected to the main branch of the tree via the fivefold- and sixfold-coordination region (denoted as 'other' minima in the following) and the overall probability for staying in the anatase region is very high. VI-a and VI-b are separated by a large energy barrier of about 0.85 eV/atom (measured from VI-a to the saddle region). Since VII-a is separated from VI-a by a barrier of only $\approx$0.013 eV/atom, energy considerations indicate that the structure should undergo a transformation into the rutile structure quite easily (even at very low temperatures). This is reflected in the fact that the probability for a transition from VII-a to VI-a is the highest one observed for MgF_2.

The structure VI-c corresponds to a half-filled NaCl structure with a ccp arrangement of anions and half the octahedral sites occupied by cations. This minimum is considerably lower in energy than VI-d, a layer structure of CdI_2 type, but the extended region surrounding VI-c contains many closely related 5- and $(5+1)$-coordinated structures as local side-minima, within an energy range of 0.30 eV/atom. The last major region of the landscape contains some structures consisting of prisms, together with a variety of other fivefold- and sixfold-coordinated structures. Except for one such 'prism' structure, they have not been used as starting minima because of their low frequency of occurrence. The one prism structure chosen (VI-e) consists of a three-dimensional network of edge- and corner-connected prisms oriented in alternating directions. In the case of VI-a, VI-c, and V-a, the energy barrier to other minima is lower than the lid value at which the first transitions to other minima are observed (see the 100% bars in figure 1(a)), indicating a relatively high entropic barrier. The relative stability is lowest for VI-d and VI-e.

The transition maps show that the anatase region is quite isolated, because only few transitions to and from this minimum are observed, and those only at relatively high energies. Minimum regions with a distinct direct connection (low relative barrier and high transition probability in at least one direction) are VII-a to VI-a, VI-d to VII-a, and VI-e to VI-c. The minimum V-a consisting of bipyramids appears to be structurally related to VI-b; but relatively few transitions are found in either direction. The transition map suggests that all side-minima would easily transform into rutile (VI-a) or anatase (VI-b) at moderate temperatures, probably via the sevenfold-coordinated structure VII-a, or the sixfold-coordinated structure VI-c, respectively.

The accessible local d.o.s. for the minimum regions of MgF_2 are plotted in figure 3(a). Quite generally, we observe a rapid exponential increase in the local d.o.s., which flattens towards higher energies, but still remains exponential on average. Thus trapping should play an important role in the dynamics. Regarding the d.o.s. in high-energy regions (>-5 eV/atom, where one can more or less assume that all minima are connected) one notes that, e.g., the slopes of VII-a and VI-d are quite similar in that energy range. This could mean that these minimum regions have a common sub-region on the energy hypersurface at high energies. Support for this hypothesis comes from the transition map, which shows that there exists a direct transition path with a high probability from VI-d to VII-a. Likewise, the d.o.s. of the minima VI-a and VI-c show a similar growth behaviour at high energies, suggesting a common region of the energy landscape, which correlates with the relatively high probability for a transition from VI-a to VI-c at higher energies.

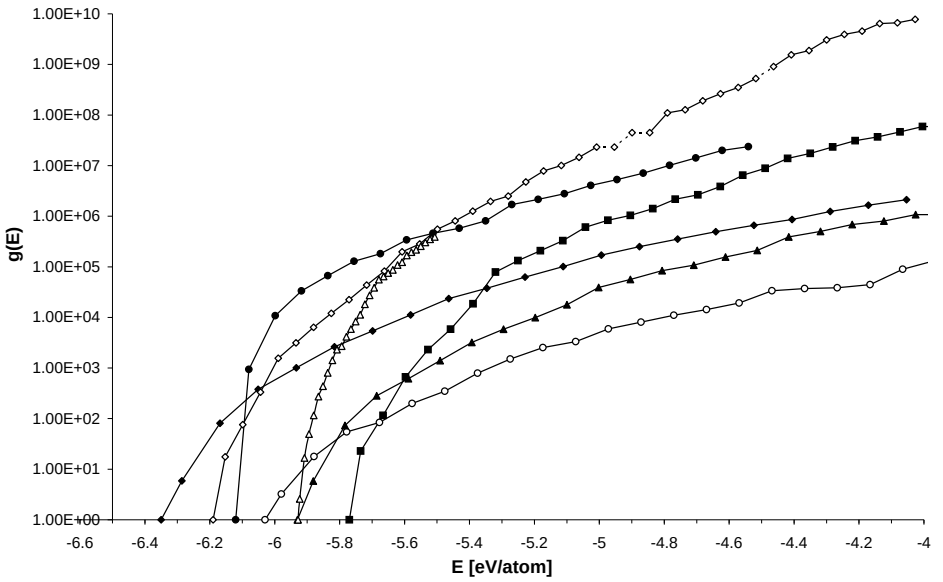

(a)

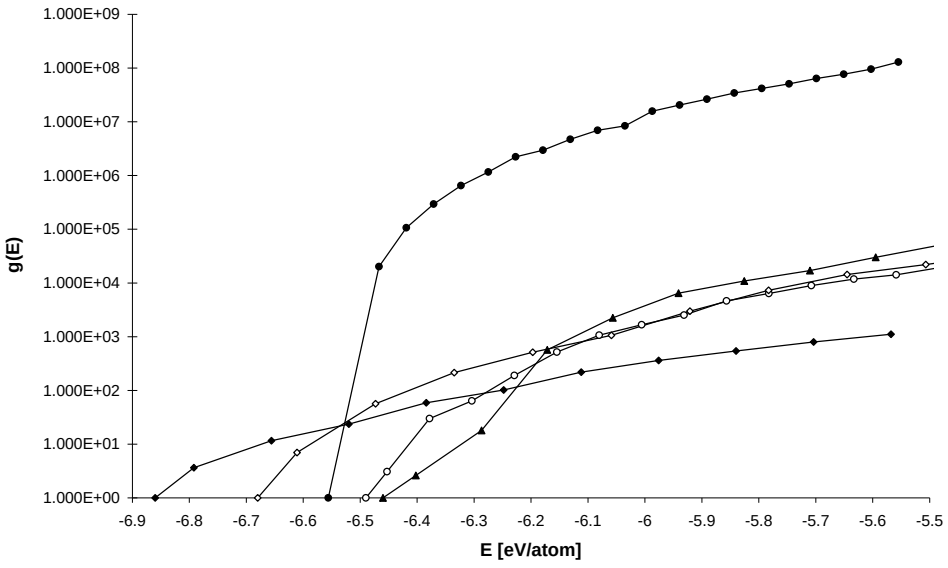

(b)

Figure 3. Local densities of states plotted on a semi-logarithmic scale. (a) MgF_2. Filled diamonds: VI-a; open diamonds: VI-b; filled circles: VII-a; open circles: VI-c; filled triangles: VI-d; open triangles: VI-e; squares: V-a. (b) CaF_2. Filled diamonds: VIII-a; open diamonds: VII-b; filled circles: VI-f; open circles: VII-c; filled triangles: VIII-b.

3.2. CaF_2

In the case of CaF_2, two variants of structures consisting of monocapped prisms (VII-b and VII-c), a distorted variant of the $CaCl_2$-type structure (VI-f), where the 'octahedra' have internal angles of less than 80° (i.e. a distortion along the trigonal axis leading to a nearly

hcp arrangement of the anions), and a structure consisting of edge- and face-connected cubes (VIII-b), were found as new local minima (cf. table 1). Here, VII-c may be interpreted as the result of a twinning of two ccp anion arrangements or as a slightly distorted CrB structure where only every second Cr position is occupied. However, no deep local minimum with high barriers analogous to the anatase structure in MgF_2 was found in CaF_2.

Compared to the case for MgF_2, the barrier structure is much simpler (cf. figure 1(b)), and the energy barriers are typically higher in the CaF_2 system (cf. the 100%-return bars in figure 1), except the barrier from VI-f to VIII-a. Analogous to the pair VII-a and VI-a in MgF_2, there is a saddle region between VI-f and VIII-a (fluorite) with a barrier far below the lowest lid at which a transition from VIII-a to any other minimum region is observed.

Overall, the most frequent transitions lead directly to VIII-a (fluorite) or VI-f, while all observed transitions leaving VIII-a occur at very high energies only, except the transition to the (energetically essentially unstable) structure VI-f (see figures 2(c)/2(d)). This probably explains why the global minimum VIII-a is more often observed in the simulated annealing runs for CaF_2 than the global minimum VI-a in MgF_2. Of all the side-minima, only VII-c exhibits no particularly frequent transition from or towards the remainder of the energy landscape. In addition, all transitions from VII-c occur at intermediate relative energy barriers (0.90–1.00 eV/atom), but the return probability is relatively high. This minimum region appears to take an intermediate position on the energy surface, being a direct neighbour to all other minima except to VI-f.

Regarding the local d.o.s. (see figure 3(b)), the VI-f minimum exhibits the largest (accessible) density of states of all minima for low lid values, like the VII-a region in MgF_2. Just as in the MgF_2 system, the deepest minimum (VIII-a) does not show the highest accessible d.o.s. during random walks for energies above -6.500 eV/atom. But, in contrast to the case for MgF_2, it does not appear possible to use the slopes of the local d.o.s. of the different minimum regions for grouping minima together.

4. Barrier structure and relaxation dynamics

The most important similarity between the related potential energy surfaces of MgF_2 and CaF_2, differing only in the cation radius, pertains to the lowest minima found, VI-a (rutile) and VIII-a (fluorite), respectively. Each corresponds to the only experimentally confirmed crystalline structure in the respective system, and VI-a and VIII-a are neighbours to very large regions in configuration space with an extremely low energy barrier, VII-a and VI-f, respectively. In both cases, the transition from the higher to the lower minimum defines the barrier, which is extremely low in energy relative to the higher minimum. In contrast, the transition in the opposite direction is the first one observed but it occurs at lids well above the actual barrier height.

Clearly, these side-minima strongly enhance the probability of reaching the global minimum during the stochastic optimization. However, the surprisingly high frequency with which VII-a was found during the simulated annealing runs indicates that there must be some features of the energy landscape that stabilize this region against VI-a. The most likely explanation is that 'entropic' barrier contributions play a role. This is supported by evidence coming from Monte Carlo runs [36] that the system finds the supposedly 'easy' exit from this region in some cases only after more than 8×10^4 steps†.

† So far, a clear definition of an 'entropic' barrier has not been agreed upon. We consider an 'entropic' barrier a measure of the difficulty of crossing (at constant energy) from region A to region B in configuration space via a random walk.

Quite generally, we observe that simple energy barriers as presented in a quasi-one-dimensional tree graph do not suffice to describe the 'difficulty' that the system encounters in finding a path along which to leave a minimum region. In order to give some quantitative feeling for the strength of the additional barriers, we have included bars for the minimum regions in the tree graph, indicating the likelihood that the system returns to the starting minimum during a threshold random walk. These bars show that many of the local minima have a stability range far exceeding that of the purely energetic barriers to a neighbouring minimum.

A similar 'entropic' stabilization appears to occur in the CaF_2 system, where structures analogous to VII-a in MgF_2 have been encountered quite often as end configurations in short quench runs. However, in the case of CaF_2 this region in configuration space does not appear to contain stable minima: after quenching for about 5×10^4 additional steps the global minimum VIII-a was always reached. On examination of long quench runs it was found that the system often lingers in this energy region for a long time, >5000 steps (cf. reference [36]), and this (metastable) region can be identified quite clearly as lying energetically between -6.74 and -6.76 eV/atom. Again this demonstrates the influence of entropic barriers on the performance of stochastic algorithms.

The major difference between CaF_2 and MgF_2 is the existence, in the MgF_2 system only, of a deep local minimum with high energetic barriers and a considerable entropic weight, which might well be able to exist: the anatase structure VI-b. But neither in real experiments nor during the optimization runs [33] is this structure easily accessible, while e.g. VII-a was found comparatively often in the simulations. We observed that out of a hundred simulated annealing runs, only 2 ended in region VI-b, while 36 ended in region VI-a, and 62 in (a total of eight) other minimum regions with energies higher than VI-b. At least regarding the results of the simulated annealing runs, we can suggest an explanation based on the analysis of the energy landscape. For one, the VI-b region is surrounded by rather high energy barriers, resulting in a high Arrhenius factor $\exp(E_B/T)$, essentially prohibiting access for temperatures below the trapping temperatures of the competing local minima. In addition, we note that the accessible local d.o.s. of the VI-b region shows approximately exponential growth, with $T_c(\text{VI-b}) \approx 0.2$ eV/atom, in the saddle region ($E \approx -5.8$–5.3 eV/atom), making it impossible to enter the pocket for $T > T_c(\text{VI-b})$. Finally, the trapping temperature in the energy range of the saddle is much lower for the anatase region than for the rest of the landscape, $T_c(\text{VI-b}) < T_c(\text{rest})$. As a consequence, by the time VI-b becomes accessible at $T = T_c(\text{VI-b})$, the system has most likely already descended into another minimum region long ago, negating the fact that e.g. $E(\text{VI-b}) < E(\text{VII-a})$, which would favour VI-b over VII-a at low temperatures. But even if we could walk at low temperatures for a nearly infinitely long time to ensure equilibration of the system, thermal equilibrium would actually favour the deepest minimum, VI-a (rutile), over VI-b (anatase)! Thus, the anatase region will not be easily accessible from the outside during Metropolis-type random walks.

To gain further insight, we have performed MC random walks at temperatures ranging from 0.001 eV/atom to 0.5 eV/atom (twenty runs for each temperature), starting at the minimum of region VI-b. At the end of each run, quenches were performed, in order to determine how the probability of returning to minimum VI-b changes as a function of temperature. The result confirms our analysis based on the results of the threshold investigations: we find a quite rapid drop in the return probability over a rather narrow temperature range around the trapping temperature $T_c(\text{VI-b})$, just as one would expect from a system that is rather abruptly released from an exponential trap. Thus, even if we had reached region VI-b during some random walk at temperatures above $T_c(\text{VI-b})$, the system would, with a high probability, leave this region again without ever getting close to the actual anatase minimum.

5. Discussion of system size effects

So far most of the work analysing continuous energy landscapes has dealt with finite clusters [14, 27], polymers [15] or proteins [10], where the whole physical system could be represented in the model. For crystalline systems, this is not possible, and the full physics and chemistry of the real crystal would only be obtainable for sizes that are for all practical (computational) purposes infinite. But many aspects of the barrier structure of the infinite system are necessarily related to that of the finite-degree-of-freedom approximation, as long as the macroscopically thermodynamically stable and metastable modifications can be represented in the finite system. As has been discussed in earlier work [37], for solids with short-range forces (including shielded Coulomb interactions) the height of the saddles (measured in eV/atom relative to the higher-lying minimum) that need to be crossed when following the minimum-energy path between two basins decreases and reaches zero in the thermodynamic limit. Here, the minimum-energy path is that route (or routes) on the landscape, along which the height of the highest saddle is as small as possible. Thus, the stability of a metastable modification of the compound will depend on the 'difficulty' of finding such a minimum-energy path, i.e. on the entropic barriers of the system represented e.g. by the transition maps and the return barriers.

From our experience with simulations of binary and ternary ionic compounds, we suggest that in many instances about eight formula units (i.e. 50–100 atoms) are sufficient to determine almost completely the most stable energetically best structures of the infinite crystal. Of course, using larger simulation cells will lead to more side-minima (for combinatorial reasons), and possibly to whole new minima basins. It is very difficult to estimate *a priori* which of these, if any, will be important for the large-scale structure of the energy surface, and the dominant transition paths. But since the structures of the deep-lying minima found for small simulation cells reappear for larger ones, independent of cell size, we expect the transitions among them to be important in larger systems as well. Of course, new alternative transition routes are likely to appear. But this will not change the qualitative aspects of the large-scale transition maps, just the quantitative values of the individual probabilities. Thus, an extensive study for at least eight formula units should represent the large-scale structure of the real energy surface at least qualitatively. Such an analysis using the threshold algorithm appears feasible with the next generation of high-speed workstation clusters.

6. Summary

Our approach to understanding the complex energy landscape of chemical systems is based on its reduction to characteristic properties. Tree-graph diagrams, which have been used in recent years as so-called 'lumped' representations of energy landscapes restrict the analysis to energy barriers. In this work, we have added transition maps that represent the probability for specific transitions between local minima, together with local densities of states, which yield further information about the energy landscapes such as the stability of minima and the general shape of the potential surface. Of particular importance is the interplay between these features of the landscape; e.g. the comparison of energetic barriers with transition maps at various energies leads to the recognition, at least in a qualitative sense, of entropic barriers in the system. From the results obtained we have gained new insights into the dynamical properties of the landscape, as seen by the correlation of the results of simulated annealing runs with the information about the landscape gleaned from energy barrier diagrams, transition probability maps, and local densities of states. Currently, these consistent results for model systems can only yield hints about the behaviour of real chemical systems. But we expect that

transferability to real compounds will be improved in the future, with rising computational power and faster algorithms for energy calculations allowing us to analyse larger systems with more precise energy functions.

Acknowledgments

We would like to thank U Burkhardt, R Hundt, and P Sibani for useful discussions. This work was partly funded by the DFG via SFB408.

References

[1] Frauenfelder H, Bishop A R, Garcia A, Perelson A, Schuster P, Sherrington D and Swart P J 1996 *Physica* D **107** 2
[2] Palmer R 1982 *Adv. Phys.* **31** 669
[3] Götze W and Sjögren J 1992 *Rep. Prog. Phys.* **55** 241
[4] Jäckle J 1986 *Rep. Prog. Phys.* **49** 171
[5] Ramakrishnan T V and Lakshmi M R (ed) 1987 *Non-Debye Relaxation in Condensed Matter* (Singapore: World Scientific)
[6] Fischer K H and Hertz J A 1991 *Spin Glasses* (Cambridge: Cambridge University Press)
[7] Sibani P 1998 *Physica* A **258** 249
[8] Bryngelson J D, Onuchic J N, Socci N D and Wolynes P G 1995 *Proteins: Struct. Funct. Genet.* **21** 167
[9] Dill K A, Bromberg S, Yue K, Fiebig K M, Yee D P, Thomas P D and Chan H S 1995 *Protein Sci.* **4** 561
[10] Onuchic J N, Luther-Schulten Z and Wolynes P G 1997 *Annu. Rev. Phys. Chem.* **48** 539
[11] Dobson C M, Sali A and Karplus M 1998 *Angew. Chem Int. Edn Engl.* **37** 868
[12] Sibani P, Schön J C, Salamon P and Andersson J-O 1993 *Europhys. Lett.* **22** 479
[13] Schön J C 1997 *J. Phys. A: Math. Gen.* **30** 2367
[14] Berry R S 1993 *Chem. Rev.* **93** 2379
[15] Becker O M and Karplus M 1997 *J. Chem. Phys.* **106** 1495
[16] Schön J C and Jansen M 1996 *Angew. Chem. Int. Edn Engl.* **35** 4001
[17] Jansen M 1996 *Abh. Rhein. Westf. Akad. Wiss.* N342
[18] Schön J C and Jansen M 1999 *Pauling's Legacy: Modern Modelling of the Chemical Bond* ed Z Maksic and W Orville-Thomas (Amsterdam: Elsevier)
[19] Berry R S and Breitengraser-Kunz R 1995 *Phys. Rev. Lett.* **74** 3951
[20] Davis H L, Wales D J and Berry R S 1990 *J. Chem. Phys.* **92** 4308
[21] Nichols J, Taylor H, Schmidt P and Simons J 1990 *J. Chem. Phys.* **92** 342
[22] Sun J-Q and Ruedenberg K 1994 *J. Chem. Phys.* **101** 2157
[23] Cerjan C J and Miller W H 1981 *J. Chem. Phys.* **75** 2800
[24] Quapp W 1996 *Chem. Phys. Lett.* **253** 286
[25] Berry R S 1994 *J. Phys. Chem.* **98** 6910
[26] Schön J C, Putz H and Jansen M 1996 *J. Phys.: Condens. Matter* **8** 143
[27] Wales D J, Miller M A and Walsh T R 1998 *Nature* **394** 758
[28] Heuer A 1997 *Phys. Rev. Lett.* **78** 4051
[29] Sibani P, van der Pas R and Schön J C 1999 *Comput. Phys. Commun.* **116** 17
[30] Sibani P and Schriver P 1994 *Phys. Rev.* B **49** 6667
[31] Schön J C and Sibani P 1998 *J. Phys. A: Math. Gen.* **31** 8167
[32] Uhlig C, Hoffmann K H and Sibani P 1995 *Z. Phys.* B **96** 409
[33] Wevers M A C, Schön J C and Jansen M 1998 *J. Solid State Chem.* **136** 233
[34] deLeeuw S W, Perram J W and Smith E R 1980 *Proc. R. Soc.* A **373** 27
[35] Metropolis N, Rosenbluth A W, Rosenbluth M N, Teller A H and Teller E 1953 *J. Chem. Phys.* **21** 1087
[36] Wevers M A C, Schön J C and Jansen M 1999 in preparation
[37] Schön J C 1998 *Proc. RIGI Workshop* ed J Schreuer (Zürich: ETH)
[38] Hundt R, Schön J C, Hannemann A and Jansen M 1999 *J. Appl. Crystallogr.* at press
[39] Hannemann A, Hundt R, Schön J C and Jansen M 1998 *J. Appl. Crystallogr.* **31** 922